

M_L Amplitude Tomography in North China

by Shunping Pei, Junmeng Zhao, Charlotte A. Rowe, Suyun Wang, Thomas M. Hearn,
Zhonghuai Xu, Hongbing Liu, and Youshun Sun

Abstract We have selected 10,899 M_L amplitude readings from 1732 events recorded by 91 stations, as reported in the Annual Bulletin of Chinese Earthquakes (ABCE), and have used tomographic imaging to estimate the lateral variations of the quality factor Q_0 (Q at 1 Hz) within the crust of Northern China. Estimated Q_0 values vary from 115 to 715 with an average of 415. Q_0 values are consistent with tectonic and topographic structure in Eastern China. Q_0 is low in the active tectonic regions having many faults, such as the Shanxi and Yinchuan Grabens, Bohai Bay, and Tanlu Fault Zone, and is high in the stable Ordos Craton. Q_0 values are low in several topographically low-lying areas, such as the North China, Taikang-Hefei, Jiangnan, Subei-Yellow Sea, and Songliao basins, whereas it is high in mountainous and uplift regions exhibiting surface expressions of crystalline basement rocks: the Yinshan, Yanshan, Taihang, Qinlin, Dabie and Wuyi Mountains, and Luxi and Jiaoliao Uplifts. Quality-factor estimates are also consistent with Pn - and Sn -velocity patterns. High-velocity values, in general, correspond with high Q_0 and low-velocity values with low Q_0 . This is consistent with a common temperature influence in the crust and uppermost mantle.

Introduction

Seismic travel-time tomography methods have enjoyed great success in the study of tectonic structure, largely because of large travel-time data sets that have been collected from regional event bulletins. Tomography can also be applied to seismic amplitude measurements; however, there are few calibrated data sets of adequate size in routine bulletins. One such data set is from the Annual Bulletin of Chinese Earthquakes (ABCE) compiled by the Institute of Geophysics of the China Earthquake Administration (IGCEA).

The ABCE amplitude data are collected for calculating event magnitudes for the M_L , m_b , m_B , and M_S magnitude scales. Over 100 stations of the Chinese network have been routinely reporting amplitudes for more than a decade. These data not only provide consistent magnitude information but are also valuable for studying regional variations in seismic attenuation.

A large body of research exists studying attenuation in China and surrounding regions using waveforms. Surface waves are often inverted for attenuation (e.g., Romanowicz *et al.*, 1995; Li *et al.*, 2000; Hong *et al.*, 2003; Gung and Romanowicz, 2004; Jemberie and Mitchel, 2004). Lg wave data have also been applied to attenuation tomography (e.g., Mitchell *et al.*, 1997; Phillips *et al.*, 2000, 2001, 2005; Cong *et al.*, 2003; Taylor *et al.*, 2003; Liu *et al.*, 2004a,b). Body waves have been collected to study attenuation (e.g., Lees and Lindley, 1994; Fan *et al.*, 2001; Rietbrock, 2001). Active seismic data are also useful for estimating attenuation

(e.g., Zhao *et al.*, 2003). Some interesting attenuation research focuses on the Tibetan Plateau (e.g., Feng and Zhou, 1985; Wu and Zeng, 1996; Reese *et al.*, 1999; Fan and Lay, 2002; Xie *et al.*, 2004).

Although some work has been conducted over broad areas to determine an averaged value or range of values for Q , little has been published using amplitude attenuation to produce detailed images of regionally varying Q . Tomographic inversion for regional imaging of Q has been performed in earlier studies using limited waveform data sets (e.g., Haberland and Rietbrock, 2001; Liu *et al.*, 2004b; Phillips *et al.*, 2005a). In this article, we present a study of tomographic attenuation in North China using a large set of amplitude data which were measured originally to calculate M_L magnitude of local and near regional events.

Data

Chinese M_L amplitudes are made following standard seismological practice, and the derived magnitudes are computed using appropriate coefficients for China (ABCE practice). The M_L magnitude is calculated from the formula $M_L = \log A\mu + R_6(\Delta)$, where $R_6 = 2.46$ for $\Delta \leq 15$ km and $R_6 = \log(\Delta) + 0.0013 \Delta + 1.27$ for $15 \text{ km} < \Delta < 1000$ km (Ge *et al.*, 1987). These M_L amplitudes are the maximum amplitudes ($A\mu$) measured on the horizontal components of short-period instruments and are used for ray

paths less than 1000 km in length. They are generally measured within the wave train that corresponds to the short-period Sg wave. At longer distances this is coincident with the longer period Lg wave train. These waves travel within the crustal wave guide and are thus sensitive to crustal variations in attenuation.

We used the M_L amplitude data of North China from the ABCE between 1985 and 1995. Most of the data are from seismograms recorded on short-period DD-1 seismographs, whose amplitude response has a frequency band of 0.5 to 20 Hz. At each station, the maximum amplitudes are the averages of the two horizontal components. Although no studies have been published regarding the uncertainties of these measurements, experienced seismologists who have used the data extensively estimate a maximum error for these values of less than 10% (Xu, 2006, personal comm.). This falls within the uncertainty estimates of our inversion, as discussed subsequently. The data were selected using the following criteria: each event was recorded by at least two stations; each station recorded at least five events; the reported period of the Sg wave at maximum amplitude is between 0.4 sec and 2.0 sec; epicentral distance is between 100 km and 800 km and event depth is less than 30 km. We finally obtained 10,899 amplitude readings from 1732 events recorded by 91 stations, as shown in Figure 1.

Method

The attenuation of seismic waves between station i and source j can be estimated from the amplitude spectrum $A_{ij}(f)$, where f is the frequency at which the amplitude is measured. Amplitude is influenced by several factors: the size of the event, station site and instrument gain, geometrical spreading, and seismic attenuation. With these, the total amplitude can be written as (e.g., Sanders, 1993; Haberland and Rietbrock, 2001):

$$A_{ij}(f) = O_j(f)S_i(f)G_{ij}(R)B_{ij}(f,R), \quad (1)$$

where $O_j(f)$ represents the event amplitude at frequency f , $S_i(f)$ is the site and instrument gain, $G_{ij}(R)$ is the geometrical spreading factor at distance R , and $B_{ij}(f)$ is seismic attenuation. The event radiation pattern has not been included. However, the maximum amplitude for Sg is produced by the interference of guided waves originating from many different sectors of the focal sphere, which tends to reduce the effect of the radiation pattern. This is reflected in the relative consistency of M_L magnitude estimates made at different seismic stations for the same event. We include frequency dependence in all terms except geometrical spreading.

We use a frequency-dependent source spectrum $O(f)$ (Brune, 1970; Hanks and Wyss, 1972) that can be described by a long-period spectral level Ω_0 and the corner frequency f_c as $O(f) = \Omega_0/(1 + (f^2/f_c^2))$. The spectral level Ω_0 is in direct proportion to the seismic moment M_0 . Frequency f and

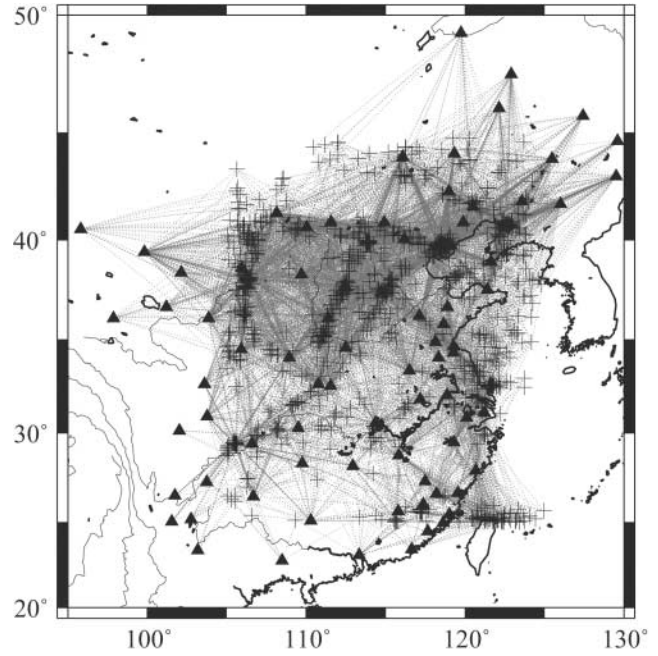


Figure 1. Distribution of ray paths, stations (triangles), and events (crosses). Gray lines represent rays from events to stations. We obtained 10,899 amplitude readings from 1732 events recorded by 91 stations.

corner frequency f_c can be considered as constants for one event, and frequency f corresponds to the frequency of the recorded waveform at maximum amplitude of Sg . We assume source spectrum $O(f)$ is frequency independent for one event, although it is variable for different events.

The site response, $S_i(f)$, includes the effect of instrument gain and site amplification. The spectral dependence of $S_i(f)$ is unknown, but the M_L bandwidth is small (0.5 Hz to 2 Hz) and the instrument response is reasonably flat within this range. We therefore assume $S_i(f)$ is also independent of frequency.

The geometrical spreading (Castro *et al.*, 1996), $G(R)$, is considered to be proportional to $(1/R)^k$, where k is the geometrical spreading coefficient, which chiefly depends on wave type. $k = 1.0$ implies spherical spreading of body waves and $k = 0.5$ represents cylindrical spreading of Lg and surface waves.

The attenuation of S waves, $B_{ij}(f)$, is attributed to the quality factor Q . We assume a frequency-dependent Q and model it as an exponential decay (e.g., Sanders, 1993; Haberland and Rietbrock, 2001):

$$B_{ij}(f) = \exp\left(-\frac{\pi f R}{vQ}\right) = \exp(-cQ_0^{-1}R), \quad (2)$$

where $c = \pi f^{1-\eta}/v$, $Q = Q_0 f^\eta$, v is the S -wave velocity, Q_0 and η are the S -wave Q at 1 Hz and its power-law frequency dependence, respectively.

Using equation (2) and taking the natural logarithm of equation (1) yields

$$Y_{ij} = \ln A_{ij}(f) - \ln G_{ij}(R) = a_i + b_j - Q_0^{-1}cR, \quad (3)$$

where the station term is $a_i = \ln S_i(f)$ and event term is $b_j = \ln O_j(f)$. Equation (3) is very similar to the Pn travel-time equation (Hearn and Ni, 1994), thereby allowing us to resolve lateral variation of Q_0 using the Pn -tomography method. We first estimate the average Q_0 by fitting the line $Y - cR$. We assume that crustal S -wave velocity is homogeneous, so rays follow a straight line. If we discretize the crust into small 2D cubes of X km by Y km, then equation (3) can be rewritten as

$$Y_{ij} = a_i - b_j - \sum_k Q_0^{-1} c R_{ijk}.$$

By subtracting Y_{ij} from the average model (fitted line), a perturbation equation can be determined as follows:

$$\Delta Y_{ij} = \Delta a_i + \Delta b_j - \sum_k \Delta Q_0^{-1} c R_{ijk}. \quad (4)$$

Equation (4) can be recast as $\mathbf{A}x = \mathbf{d}$, where \mathbf{d} is the data vector, x is the vector of unknowns, and \mathbf{A} represents the model parameters. We apply damped LSQR (Paige and Saunders, 1982) with preconditioning to find the least-squares solution. Laplacian smoothing was applied in the inversion (Lees and Crosson, 1989).

Results

A geometrical spreading coefficient (k) of 1.0 is selected, because the standard deviation of the observation residuals (ΔY_{ij}) in equation (4) is smaller for $k = 1.0$ than $k = 0.5$. We take the average Q -decay coefficient (η) of 0.5 (Liu *et al.*, 2003), and the crustal velocity (v) of 3.6 km/sec, which was determined from Sg -wave travel times. By fitting a straight line to the data set of M_L amplitude (Y_{ij}) versus reduced epicentral distance (cR) according to equation (3), we obtain an average S -wave Q_0 of 415 from the slope. We discretize the crust into blocks with cell dimensions of $15' \times 15'$, and adopt a damping constant of 1000. The S -wave Q_0 lateral variations, the station term, and the event term perturbations are obtained by tomographic inversion of the M_L amplitude residuals after 60 iterations. Figure 2 shows the resulting lateral variations of the S -wave quality factor Q_0 , which varies from 115 to 715. Blue corresponds to a high-quality factor (low attenuation) and red corresponds to a low-quality factor (highly attenuative crust).

The station term perturbations Δd_i and event term perturbations Δb_j are shown in Figure 3. Negative station term perturbations represent large attenuation beneath the station and positive perturbation represents small attenuation. A station term of 1.0 represents an amplitude gain factor of $e^{1.0}$ or 2.73. A few stations have gains greater than this, but most

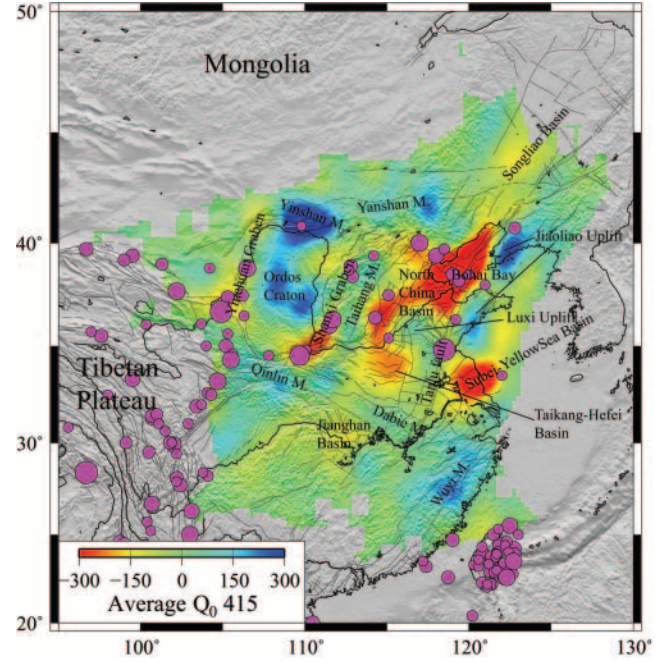


Figure 2. Imaged Q_0 lateral variations. Blue corresponds to a high value and red corresponds to low. Average Q_0 is 415 and varies from 115 to 715. Lines represent active faults; magenta circles represent earthquakes having magnitudes greater than 7.0 (Wang *et al.*, 2003). Q_0 is low in the active tectonic areas with many faults, such as the Shanxi and Yin-chuan Grabens, Bohai Bay, and Tanlu Fault Zone. Q_0 is also low in several basins, including the North China Basin, Taikang-Hefei Basin, Jiangnan Basin, Subei-Yellow Sea Basin, and Songliao Basin. High Q_0 occurs both in the stable Ordos Craton and in all mountains and uplift regions where crystalline basement appears at the surface, such as Yinshan, Yanshan, Taihang, Qinlin, Dabie and Wuyi Mountains, and Luxi and Jiaoliao Uplifts.

stations have gains near one. An event term of 1.0 represents a magnitude bias of $\log_{10} e^{1.0}$ or 0.43 magnitude units. Events with gray squares have larger source sizes than the magnitudes indicated; the discrepancies are caused by the higher attenuation regions shown in Figure 2.

Residuals between -2 and $+2$ are used in the tomographic inversion. The standard deviation of the residuals is reduced from 0.67 to 0.41 after inversion (Fig. 4). Checkerboard tests were employed to analyze the spatial resolution of our solution. For the given ray paths in this study, theoretical amplitude residuals were calculated for input ΔQ_0 models with ± 300 in different square sizes. Gaussian random noise with zero mean and a standard deviation of 0.41 was added to the calculated residuals. Then the synthetic amplitude residuals were inverted to determine whether the squares could be resolved. Figure 5a, b shows checkerboard test models with cell size of 2° by 2° and 1.5° by 1.5° , respectively. The tests indicate that tomogram resolution is on the order of 2° in most regions and 1.5° in the North China

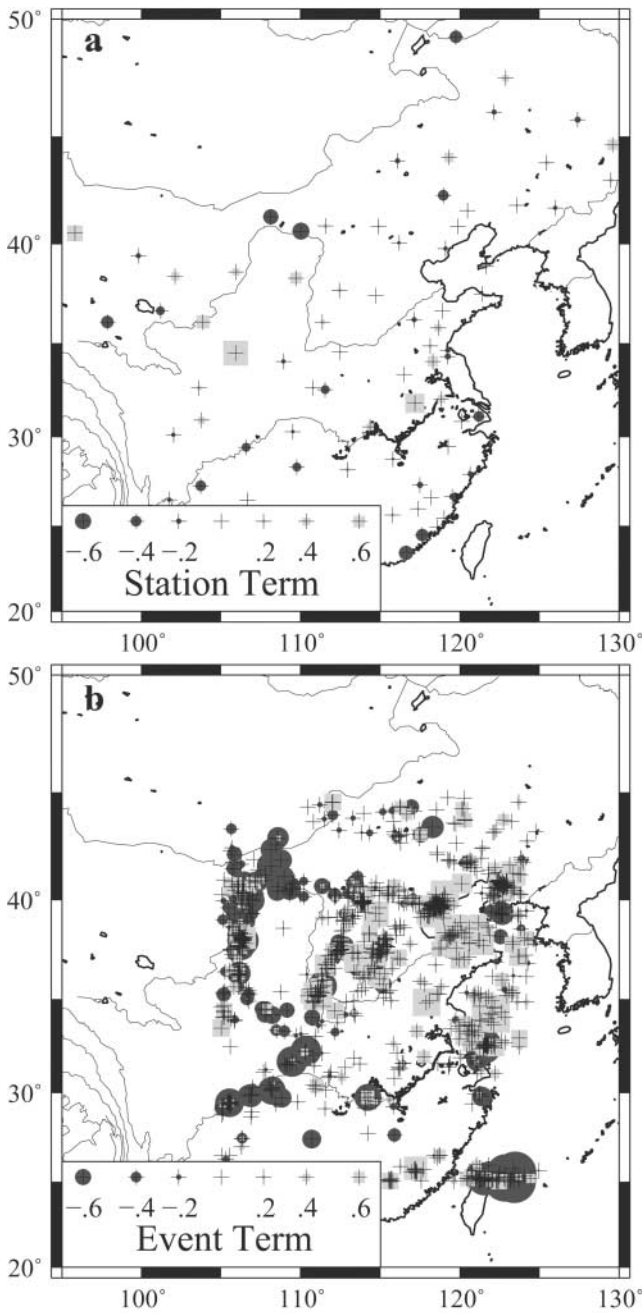


Figure 3. Station term perturbations Δa_i (a) and event term perturbations Δb_j (b). Negative station term perturbations represent large attenuation beneath the station, and positive perturbation represents small attenuation. A station term of 1.0 represents an amplitude gain factor of $e^{1.0}$ or 2.73. A few stations have gains greater than this, but most stations have gains near one. An event term of 1.0 represents a magnitude bias of $\log_{10} e^{1.0}$ or 0.43 magnitude units. Events with gray squares have larger source sizes than the magnitudes indicated; the discrepancy arises from rays passing through the higher attenuation regions shown in Figure 2.

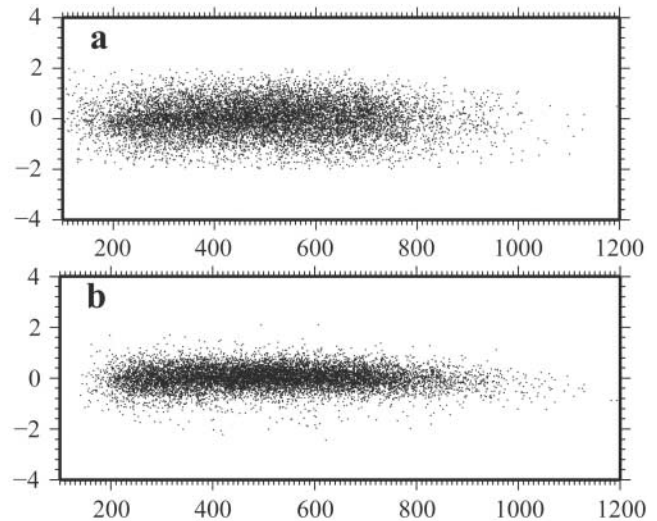


Figure 4. Distribution of amplitude residuals versus reduced epicentral distance (cR) before inversion (a) and after inversion (b). Residuals between -2 and $+2$ are used in the tomographic inversion. The standard deviation of the residuals is reduced from 0.67 to 0.41 after inversion.

Basin. A random error of up to 0.41 can be effectively damped through application of these inversion parameters. Our checkerboard test indicates that the amplitude data errors of 10% have little influence on the resulting Q values.

Discussion

Figure 2 shows that the quality factor is consistent with the tectonic structure in North China. Most large earthquakes occur in the low- Q regions, consistent with an intuitive expectation of a strong correlation between greatest seismicity and highly attenuative crust. Low Q_0 follows active tectonic areas having many faults, such as the Shanxi and Yinchuan Graben, Bohai Bay, and Tanlu Fault Zone, whereas Q_0 is high in the stable Ordos Craton. This elevated attenuation can be attributed to the greater scattering and/or absorption in the fractured or faulted zone, compared with intact rocks. At the same time, the Q_0 is consistent with topography in Eastern China. Q_0 is low in some large basins such as the North China Basin, Taikang-Hefei Basin, Jiangnan Basin, Subei-Yellow Sea Basin, and the Songliao Basin. High Q_0 occurs in most mountains and uplift regions where crystalline basement appears at the surface, including the Yinshan, Yanshan, Taihang, Qinlin, Dabio and Wuyi Mountains, Luxi and Jiaoliao Uplifts. Oil and/or gas were found in all basins mentioned previously, and Mesozoic and older rocks are ubiquitous in the mountain areas and uplift regions mentioned (Ma, 1989; Steinshouer *et al.*, 1999). Low Q_0 observed in the basins may result from fluid-filled cracks and pores in the upper crust and deep sedimentary basins. The average depth of earthquakes in our research area is 13 km, and the densest ray coverage is thus within about 6–7 km

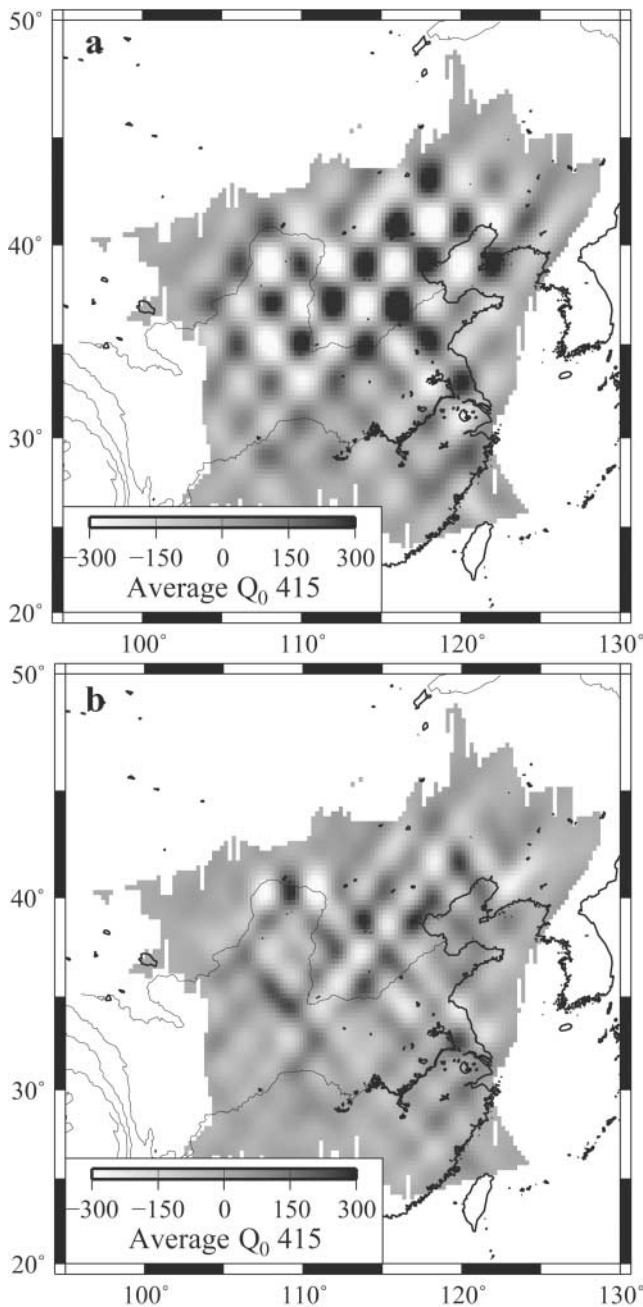


Figure 5. Output quality-factor model created from a checkerboard test model with cell sizes of 2° by 2° (a) and 1.5° by 1.5° (b). Gaussian random noise with zero mean and a standard deviation of 0.41 is added to the calculated residuals. The tests indicate that tomogram resolution is on the order of 2° in most regions and 1.5° in the North China basin.

depth, so the results of the inversion primarily address Q_0 lateral variations within the uppermost 6–7 km of the crust, where oil is typically found. Temperature may also be an important factor in the Q_0 pattern because the Earth's heat flow is high in basins and low in mountains and uplift regions in eastern China (Hu *et al.*, 2001; Wang *et al.*, 2003).

High-attenuation values in the North China Basin were observed by Liu *et al.* (2004b) and Phillips *et al.* (2005a). Our results are consistent with these earlier studies, but provide higher resolution and more detailed information in the North China Basin, Shanxi and Yinchuan Grabens, Ordos Craton, and surrounding regions.

Our estimate of the quality factor is also consistent with previously determined patterns of P_n (Wang *et al.*, 2003; Hearn *et al.*, 2004; Liang *et al.*, 2004; Sun *et al.*, 2004; Phillips *et al.*, 2005b; Sun and Toksöz, 2006) and S_n velocities (Pei *et al.*, 2004). High velocity almost always corresponds with high Q_0 and low velocity with low Q_0 , possibly because of common temperature influence in the crust and uppermost mantle.

Most event terms shown in Figure 3 have values between -1 and 1 and are geographically correlated. An event term of 1.0 corresponds to a $\log_{10}(2.73) = 0.43$ change in magnitude. This suggests that the M_L for events in central North China systematically underestimate the event size by almost one-half of a magnitude unit, whereas events in Taiwan, the southeast China coast, and west of Ordos systematically overestimate the size by almost one-half of a magnitude unit.

Station terms vary less than event terms, but some still show values of up to 1.0 . A station term of 1.0 suggests an amplification gain factor of 2.73 for the station because of site response and instrument gains. There are few stations with this amount of amplification; these have only a few data points associated with them. Furthermore, there is no geographical consistency between the station terms. We infer from this that station site amplification for the ABCE is not an important effect.

We analyzed the sensitivity of parameters, such as Q decay coefficient η , geometrical spreading coefficient k and S -wave velocity v . We found that the pattern of relative Q_0 lateral variations is very stable, although absolute Q_0 may change with different parameters. Less than 20% variation of absolute Q_0 will be produced if η varies between 0.3 and 0.9, and v varies between 3.3 and 3.9 km/sec.

Conclusions

This study uses tomographic imaging to investigate crustal attenuation beneath Northern China. Variations in attenuation are large enough that the standard M_L magnitude calculation can estimate event source size incorrectly by as much as one-half of a magnitude unit. We find that attenuation levels are correlated with regional tectonic structure. High attenuation often occurs in active tectonic areas with significant faulting, whereas attenuation is low in the stable Ordos Craton. The estimate of attenuation shows a close correlation with topography. Q_0 is generally low in basins, whereas high Q_0 mostly occurs in mountains and uplift regions where crystalline basement appears at the surface. It is possible that low Q_0 in basins is caused by fluid in the upper crust, high heat flow, and/or deep sediment in basins,

whereas high Q_0 in the mountains and uplift regions results from the presence of old, dense, competent rock and low heat flow. The quality factor is also consistent with Pn - and Sn -velocity patterns. High velocity generally corresponds with high Q_0 and low velocity with low Q_0 , possibly because of a common temperature influence in the crust and uppermost mantle.

Acknowledgments

We sincerely thank Guomin Zhang, Jie Liu, and Shenghong Tai for their support and helpful suggestions to this study. We also thank Jonathan Ajo-Franklin, Margaret Benoit, Xander Campman, and Burke Minsley for their valuable comments in improving the manuscript. We are grateful to Anton M. Dainty and an anonymous reviewer for their constructive comments and suggestions. This research was supported jointly by the Talent Project of the Chinese Academy of Sciences (CAS), the Knowledge Innovating Project of the CAS (Grant No. kzcx3-sw-143), the Earth Resources Laboratory at Massachusetts Institute of Technology (under Contract No. FA8718-04-C-0018), and Los Alamos National Laboratory, U.S. Department of Energy, as Publication No. LAUR-06-2435.

References

- Brune, J. N. (1970). Tectonic stress and the spectra of seismic shear waves from earthquakes, *J. Geophys. Res.* **75**, 4997–5009.
- Castro, R., F. Pacor, A. Sala, and C. Petrangaro (1996). S wave attenuation and site effects in the region of Friuli, Italy, *J. Geophys. Res.* **101**, 22,355–22,369.
- Cong, L. L., J. F. Hu, Z. W. Fu, Y. B. Wen, G. F. Kang, and X. P. Wu (2003). Distribution of Lg coda Q in the Chinese continent and its adjacent regions, *Science in China Ser. D* **46**, 529–539.
- Fan, G., and T. Lay (2002). Characteristics of Lg attenuation in the Tibetan Plateau, *J. Geophys. Res.* **107**, no. B10, 2256, doi 10.1029/2001JB000804.
- Fan, J. C., S. L. Li, X. L. Lai, and H. Z. Deng (2001). Three-dimensional Q structure in Jiashi earthquake region of Xinjiang region, *Acta Seism. Sinica* **24**, 573–581 (in Chinese).
- Feng, R., and H. N. Zhou (1985). Crustal Q structure beneath the Tibetan Plateau, *Chin. J. Geophys.* **28** (Suppl.), 174–184 (in Chinese).
- Ge, H. C., C. Z. Huang, P. Y. Ye, and Z. F. Lu (1987). Lg magnitude determination for the eastern six provinces of China (part I): method and results, *Acta Seism. Sinica* **9**, 37–51 (in Chinese).
- Gung, Y., and B. Romanowicz (2004). Q tomography of the upper mantle using three-component long-period waveforms, *Geophys. J. Int.* **157**, 813–830.
- Haberland, C., and A. Rietbrock (2001). Attenuation tomography in the western central Andes: a detailed insight into the structure of a magmatic arc, *J. Geophys. Res.* **106**, 11,15–11,167.
- Hanks, T. C., and M. Wyss (1972). The use of body-wave spectra in the determination of seismic-source parameters, *Bull. Seism. Soc. Am.* **62**, 561–589.
- Hearn, T. M., and J. Ni (1994). Pn velocities beneath continental collision zones, the Turkish-Iranian plateau, *Geophys. J. Int.* **117**, 273–283.
- Hearn, T. M., S. Wang, J. F. Ni, Z. Xu, Y. Yu, and X. Zhang (2004). Uppermost mantle velocities beneath China and surrounding regions, *J. Geophys. Res.* **109**, no. B11301, doi 10.1029/2003JB002874.
- Hong, X. H., J. S. Zhu, J. M. Cao, and Z. Q. Xu (2003). Tomography of 3-D S-wave quality factor of the crust and upper mantle in China, *Chin. J. Geophys.* **46**, 642–651 (in Chinese).
- Hu, S. B., L. J. He, and J. Y. Wang (2001). Compilation of heat flow data in the China continental area (3rd edition), *Chin. J. Geophys.* **44**, 612–626 (in Chinese).
- Jemberie, A. L., and B. J. Mitchell (2004). Shear wave Q structure and its lateral variation in the crust of China and surrounding regions, *Geophys. J. Int.* **157**, 363–380.
- Lees, J. M., and R. S. Crosson (1989). Tomographic inversion for three-dimensional velocity structure at mount St. Helens using earthquake data, *J. Geophys. Res.* **94**, 5716–5728.
- Lees, J. M., and G. T. Lindley (1994). Three-dimensional attenuation tomography at Loma Prieta: Inversion of t^* for Q, *J. Geophys. Res.* **99**, 6843–6863.
- Li, G. P., G. M. Xu, E. G. Gao, and Y. Xu (2000). Q_β Tomography under the crust and upper mantle in Eastern China, *Acta Seism. Sinica* **22**, 73–81 (in Chinese).
- Liang, C., X. Song, and J. Huang (2004). Tomographic inversion of Pn travel times in China, *J. Geophys. Res.* **109**, B11304, doi 10.1029/2003JB002789.
- Liu, J., S. H. Zheng, and Y. L. Huang (2003). The inversion of non-elasticity coefficient, source parameters, site response using Genetic Algorithms, *Acta Seism. Sinica* **25**, 211–218 (in Chinese).
- Liu, J. H., F. T. Liu, X. W. Yan, Y. Xu, and T. Y. Hao (2004a). A study of Lg attenuation in North China—the measurement of Lg coda Q, *Chin. J. Geophys.* **47**, 822–831 (in Chinese).
- Liu, J. H., F. T. Liu, X. W. Yan, Y. Xu, and T. Y. Hao (2004b). A study of Lg coda attenuation beneath North China: seismic imaging of Lg Coda Q_0 , *Chin. J. Geophys.* **47**, 1044–1052 (in Chinese).
- Ma, X. Y., ed. (1989). *Lithospheric Dynamics Atlas of China*, China Cartographic Publishing House, Beijing (in Chinese).
- Mitchell, B. J., Y. Pan, J. Xie, and L. Cong (1997). Lg coda Q variation across Eurasia and its relation to crustal evolution, *J. Geophys. Res.* **102**, 22,767–22,779.
- Paige, C. C., and M. A. Saunders (1982). LSQR, An algorithm for sparse linear equations and sparse linear system, *ACM Trans. Math. Software* **8**, 43–71.
- Pei, S. P., Z. H. Xu, and S. Y. Wang (2004). Sn wave tomography of the uppermost mantle beneath the China continent and adjacent regions, *Chin. J. Geophys.* **47**, 278–284.
- Phillips, W. S., H. E. Hartse, S. R. Taylor, and G. E. Randall (2000). 1 Hz Lg Q tomography in central Asia, *Geophys. Res. Lett.* **27**, 3425–3428.
- Phillips, W. S., H. E. Hartse, S. R. Taylor, A. A. Velasco, and G. E. Randall (2001). Application of regional phase amplitude tomography to seismic verification, *Pure Appl. Geophys.* **158**, 1189–1206.
- Phillips, W. S., H. E. Hartse, and J. T. Rutledge (2005a). Amplitude ratio tomography for regional phase Q, *Geophys. Res. Lett.* **32**, doi 10.1029/2005GL023870.
- Phillips, W. S., C. A. Rowe, and L. K. Steck (2005b). The use of interstation P wave arrival time differences to account for regional path variability, *Geophys. Res. Lett.* **32**, L11301, doi 10.1029/2005GL022558.
- Reese, C. C., R. R. Rapine, and J. F. Ni (1999). Lateral variation of Pn and Lg attenuation at the CDSN station LSA, *Bull. Seism. Soc. Am.* **89**, 325–330.
- Rietbrock, A. (2001). P wave attenuation structure in the fault area of the 1995 Kobe earthquake, *J. Geophys. Res.* **106**, 4141–4154.
- Romanowicz, B. (1995). A global tomographic inversion model of shear attenuation in the upper mantle, *J. Geophys. Res.* **100**, 12,375–12,394.
- Sanders, C. O. (1993). Local earthquake tomography: attenuation theory and results, in *Seismic Tomography: Theory and Practice*, H. Iyer and K. Hirahara (Editors), Chapman and Hall, New York, 676–694.
- Steinshouer, D. W., J. Qiang, P. J. McCabe, and R. T. Ryder (1999). Maps showing geology, oil and gas fields, and geologic provinces of the Asia pacific region, *U.S. Geol. Surv. Open-File Rept.* 97-470F.
- Sun, Y., and M. N. Toksoz (2006). Crustal structure of China and surrounding regions from P-wave travel-time tomography, *J. Geophys. Res.* **111**, B03310, doi 10.1029/2005JB003962.
- Sun, Y., L. Xu, S. Kuleli, F. D. Morgan, and M. N. Toksoz (2004). Adaptive moving window method for 3-D P-velocity tomography and its application in China, *Bull. Seism. Soc. Am.* **94**, 740–746.
- Taylor, S. R., X. Yang, and W. S. Phillips (2003). Bayesian Lg Attenuation Tomography Applied to Eastern Asia, *Bull. Seism. Soc. Am.* **93**, 795–803.

- Wang, S. Y., Z. H. Xu, and S. P. Pei (2003). Velocity structure of uppermost mantle beneath North China from Pn tomography and its implications, *Sci. China Ser. D* **46** (Suppl.), 130–140.
- Wu, J. P., and R. S. Zeng (1996). Inversion of Q value structure beneath the Tibet plateau, *Acta Seism. Sinica* **18**, 208–214 (in Chinese).
- Xie, J., R. Gok, J. Ni, and Y. Aoki (2004). Lateral variations of crustal seismic attenuation along the INDEPTH profiles in Tibet from Lg Q inversion, *J. Geophys. Res.* **109**, B10308, doi 10.1029/2004JB002988.
- Zhao, J. M., X. K. Zhang, H. Z. Deng, and J. Zhang (2003). Q value structure of the upper crust along the geoscience transect from Baicheng to Da Qaidam, *Chin. J. Geophys.* **46**, 725–735.

Institute of Tibetan Plateau Research
Chinese Academy of Sciences
Beijing 100085, China
(S.P., J.Z., H.L.)

Los Alamos National Laboratory
Los Alamos, New Mexico 87545
(C.A.R.)

Institute of Geophysics
China Earthquake Administration
Beijing 100081, China
(S.W., Z.X.)

New Mexico State University
Physics Department
Las Cruces, New Mexico 88003
(T.M.H.)

Earth Resources Laboratory
Massachusetts Institute of Technology
Cambridge, Massachusetts 02139
(Y.S.)

Manuscript received 21 January 2006.